SoftwareX 23 (2023) 101481

Contents lists available at ScienceDirect

SoftwareX

journal homepage: www.elsevier.com/locate/softx

Original software publication

voxTrace: A voxel-based Monte-Carlo ray-tracing code for the simulation of X-ray fluorescence spectra

Michael Iro [a,*], Dieter Ingerle [b], Sven Hampel [c], Ursula Fittschen [c], Vishal Dhamgaye [d], Oliver Fox [d], Christina Streli [a]

[a] Atominstitut, TU Wien, Stadionallee 2, 1020 Vienna, Austria
[b] X-ray center, TU Wien, Getreidemarkt 9, 1060 Wien, Austria
[c] Clausthal University of Technology, Institute of Inorganic and Analytical Chemistry, Arnold-Sommerfeld-Str. 4, 38678 Clausthal-Zellerfeld, Germany
[d] Diamond Light Source, Harwell Science and Innovation Campus, Didcot, OX11 0DE, UK

ARTICLE INFO

Article history:
Received 16 May 2023
Received in revised form 7 July 2023
Accepted 17 July 2023

Keywords:
Monte-Carlo
Ray-tracing
X-ray fluorescence
Simulation
Quantification
Confocal XRF

ABSTRACT

Confocal micro-X-ray fluorescence analysis (CMXRF), using polycapillary optics, is a powerful technique for the non-destructive investigation of the three-dimensional elemental distribution of samples from many different research areas, including biology, cultural heritage and material science. To solve the problem of the quantitative interpretation of CMXRF measurements, voxTrace introduces a new fundamental Monte-Carlo ray-tracing approach, to simulate the measured spectra. This enables the consideration of effects such as secondary excitation, elastic and inelastic scattering. Furthermore, measurements with step sizes between measurement points smaller than the average confocal volume can be interpreted without complicated sample reconstruction algorithms. Solving this problem of high computational effort, in reasonable timescales, is made feasible by the effective use of graphics processing units (GPU) with CUDA.

Code metadata

Current code version	*1.0.0*
Permanent link to code/repository used for this code version	https://github.com/ElsevierSoftwareX/SOFTX-D-23-00323
Permanent link to reproducible capsule	
Legal code license	*MIT License*
Code versioning system used	*git*
Software code languages, tools and services used	*C++, C, CUDA*
Compilation requirements, operating environments and dependencies	*Ubuntu 22.04 cuda gcc armadillo* autoconf automake autotools-dev build-essential cmake g++ gfortran gnuplot libarmadillo-dev libboost-dev libgsl-dev libhdf5-dev libtool meson ninja-build pkg-config python3 python3-dev python3-pip python3-setuptools python3-wheel sed wget xraylib shadow3 polycap sciplot ensmallen easyRNG
If available, link to developer documentation/manual	https://michaeliro.github.io/voxTrace/
Support email for questions	michael.iro@tuwien.ac.at

1. Motivation and significance

Confocal micro-X-ray fluorescence analysis (CMXRF) is a widely used technique for the non-destructive investigation of the three-dimensional elemental distribution ("imaging") of various samples [1–3]. At present, the quantitative interpretation of such measurements still poses a problem in research, as there are many parameters which must be included. Solutions must be found iteratively, as no closed-form solution for this complex problem is possible. The energy dependent attenuation of X-rays in the sample, which is often of inhomogeneous composition, must be considered, as well as the, also energy dependent, transmission properties of the X-ray optics (for example, polycapillary optics) used in the setup [4]. While other approaches use analytical estimations for the transmission properties of the polycapillary optics and the energy-dependent confocal volume investigated [5], voxTrace introduces a fundamental ray-tracing

* Corresponding author.
E-mail address: michael.iro@tuwien.ac.at (Michael Iro).

https://doi.org/10.1016/j.softx.2023.101481

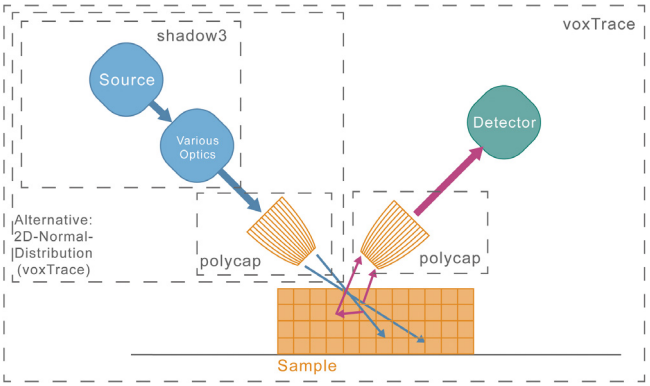

Fig. 1. Schematic drawing of a modelled experimental setup, showing the different software packages used for modelling the different components of the setup. Primary X-rays (blue) interact with material in the sample (absorption and scattering), producing secondary X-rays (red), which can again interact with the sample. (For interpretation of the references to colour in this figure legend, the reader is referred to the web version of this article.)

approach to address the problem. This approach poses many advantages, such as an energy-independent voxel size, instead of a voxel size determined by the energy dependent confocal volume, and the simulation of higher order effects (such as secondary excitation).

The commonly used and freely available software packages shadow3 [6] and polycap [7] can be used to simulate the properties of an X-ray beam generated by synchrotron sources and manipulated with X-ray optics routinely available on beamlines, including polycapillary optics. The rays generated in these simulations are then traced through a sample with a voxel-size independent of the confocal volume and further through a second polycapillary optic in collecting mode. The energies of the rays, reaching the detector can be displayed as an energy dispersive spectrum and compared with measured spectra, without the intermediate step of peak deconvolution (see Fig. 1).

2. Software description

2.1. Software architecture

Initial implementation attempts with C++ and OpenMP proved to be inadequate in terms of computational speed, when tackling this computationally demanding, but pleasingly parallel ray-tracing problem. Graphics processing units (GPUs) are a natural candidate as a hardware setup in this context. Therefore, the software was implemented using NVIDIA's CUDA C++ toolkit.

To obtain a flexible, expandable, comprehensible and easily maintainable code an object-oriented approach was chosen. The objects are as follows: ChemElementGPU, MaterialGPU, VoxelGPU, SampleGPU, RayGPU and TracerGPU.

ChemElementGPU discretizes fundamental parameters for the interaction of X-rays with matter, taken from xraylib [8,9]. For memory efficiency only one ChemElementGPU is instantiated for each chemical element contained in the sample. To separate geometrical and X-ray-matter interactions, the class MaterialGPU, holds pointers to the above-mentioned ChemElementGPUs and their respective weights. VoxelGPU holds all geometrical information about the voxel, including its nearest neighbours and a pointer to its MaterialGPU. SampleGPU holds all voxels and a specified Out-Of-Bounds-Voxel. RayGPU has the member variables for starting coordinates, direction and energy. TracerGPU is used to instantiate all classes and allocate the according memory on the graphics unit. A class-diagram of the structure which aims to find a balance between memory efficiency and performance is shown in Fig. 2.

2.2. Software functionalities

Given the spatial distribution of the composition of a sample material and the modelling parameter of the experimental setup (X-ray source, polycapillary optics and distances), voxTrace can be used to simulate the measured signal in reasonable time. The simulation process follows the path of primary and secondary X-rays, produced in the follow-up process of interactions of the primary X-rays with matter, through a sample. It begins with an X-ray exiting the primary polycapillary exit window. The parameters for the primary X-rays, including starting coordinates, direction and energy, can be taken from a list previously generated and traced with shadow3 [6], to model various sources and optics, and polycap [7], to model the path through the primary polycapillary optic. Alternatively, voxTrace offers the option of generating beams coming from the polycapillary optic. Using shadow3 [6] and polycap [7] allows the exact modelling of complex systems, such as synchrotron sources, mirrors and monochromator optics. However, the process of reading large files can significantly decrease the performance of the program, for example in our case a primary beam of roughly 7 TB was necessary to simulate a statistically relevant signal. Therefore, the option to generate 2D-Gaussian distributed rays, as a primary beam, provides a considerable speed advantage. Previous research has shown that a 2D normal distribution accurately approximates the spatial distribution of X-rays focussed by a polycapillary half-lens optic [4].

The fundamentals for Monte-Carlo ray-tracing of X-rays in a sample have been expertly discussed by Vincze et al. and Schoonjans et al. in a series of papers [10–14]. An overview of the process and its implementation in this voxel-based setup, with secondary optics is given below. For the fundamental parameters, such as attenuation coefficients, densities, and radiative rates, data is taken from xraylib [8,9] and discretized in the ChemElementGPU class.

The first step involves searching the first voxel of the sample model with an intersection with the given ray. If none is found a new ray is generated or taken from the list. Once the voxel has been identified, the intersection length between voxel and ray and the total linear attenuation coefficient can be calculated. The decision whether an interaction takes place in the voxel or not is made using Beer's law, describing the attenuation of radiation in matter.

$$I_x = I_0 \cdot e^{-\mu \cdot \Delta x}$$

where I_x is the intensity of the attenuated beam, I_0 the intensity of the primary beam, μ the linear attenuation coefficient and Δx the intersection length of the ray and the voxel. Thus, the probability of an interaction in this voxel as a number between 0 and 1 can be written as $e^{-\mu \cdot \Delta x}$. Whether an interaction takes place is then calculated by comparing this value with a random number R between 0 and 1. In the following steps a new random number R is generated for each step.

$$e^{-\mu \cdot \Delta x} < R = \begin{cases} true \rightarrow Interaction \\ false \rightarrow go\ to\ next\ Voxel \end{cases}$$

Which of the chemical elements interacts with the given ray is calculated by the comparison of a random number R between 0 and 1 with the ratio of the attenuation coefficient of the mass proportion of each element in the material to the total attenuation coefficient of the material $\mu_{i-Lin-\%}$.

$$\sum_{i}^{k} \mu_{i-Lin-\%} \leq R \leq \sum_{i}^{k+1} \mu_{i-Lin-\%}$$

where $\mu_{i-Lin-\%} = \frac{w_i \cdot \mu_{Lin-i}}{\mu_{Lin-Total}}$, μ_{Lin-i} is the linear absorption coefficient of the element i with a given weight fraction w_i of the

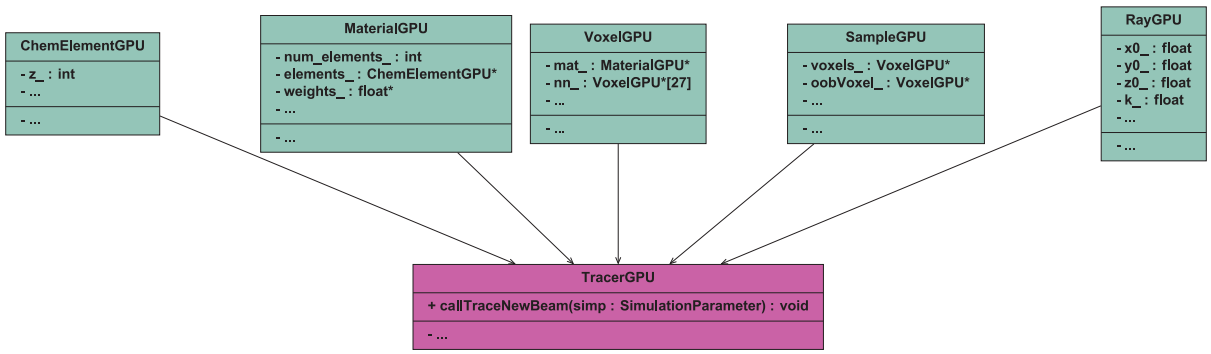

Fig. 2. Class-diagram of voxTrace main classes. The architecture, minimizing the amount of redundantly stored information about the fundamental parameters of chemical elements aims to find a balance between memory efficiency and performance.

element in the material of the voxel, a total linear attenuation coefficient $\mu_{Lin-Total}$ and k being a number smaller than the number of elements in the material.

The type of interaction is established by a comparing a random number R between 0 and 1 with the ratios of the sum of the cross-sections for photo absorption $\tau\,(E)$, Rayleigh scattering $\sigma_R\,(E)$ and Compton scattering $\sigma_C\,(E)$ with the total attenuation cross-section $\mu\,(E)$.

$$0 \leq R \leq \frac{\tau\,(E)}{\mu\,(E)} \rightarrow \; Photo - absorption$$

$$\frac{\tau(E)}{\mu(E)} \leq R \leq \frac{\tau\,(E) + \sigma_R\,(E)}{\mu\,(E)} \rightarrow Rayleigh\ scattering$$

$$\frac{\tau(E) + \sigma_R(E)}{\mu(E)} \leq R \leq \frac{\tau\,(E) + \sigma_R\,(E) + \sigma_C\,(E)}{\mu\,(E)} = 1 \rightarrow Compton\ Scattering$$

In case of photo-absorption, the interacting shell is established using the photo-absorption cross-section $\tau_i\,(E)$ for a single shell ionization i of the element.

$$\sum_i^k \frac{\tau_i\,(E)}{\sum_j \tau_j\,(E)} \leq R \leq \sum_i^{k+1} \frac{\tau_i\,(E)}{\sum_j \tau_j\,(E)}$$

with $\sum_j \tau_j\,(E)$ being the total photo absorption cross-section of the element.

The relaxation process of the excited atom is established by the comparison of the fluorescence yield ω_i of an excited shell i with a new random number R between 0 and 1.

$$\omega_i > R = \begin{cases} true \;\rightarrow Fluorescence\ Photon \\ false \rightarrow Auger\ Electron \end{cases}$$

In the case of relaxation via Auger electron emission, a new ray is generated. In the case of a fluorescence photon emission, its characteristic energy is established, with the use of the radiative rates r_i of a transition i.

$$\sum_i^k r_i \leq R \leq \sum_i^{k+1} r_i$$

The direction of the secondary ray (scattered or fluorescence) can be calculated using random numbers and the differential Rayleigh scattering and Compton scattering. Fig. 3 shows the rotational angles ϕ and ϑ necessary for calculation of the direction of the secondary ray.

For fluorescence photons, ϕ and ϑ can be calculated using random numbers R between 0 and 1.

$$\phi = 2\pi R$$

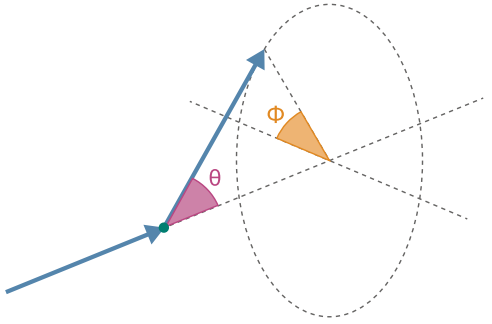

Fig. 3. Coordinate transformation of a ray during an interaction process (scattering or fluorescence). The angles ϕ and ϑ are established using the differential scattering cross-sections for Rayleigh scattering and Compton scattering and random numbers.

$$\vartheta = \text{acos}(2R - 1)$$

While the calculation of ϕ is the same for scattered photons, the ϑ of an elastic or inelastic scattered ray is calculated using the differential scattering cross-sections for Rayleigh scattering or Compton scattering, respectively.

$$\frac{2\pi}{\sigma\,(E,Z)} \sum_o^i \frac{d\sigma}{d\Omega}\,(E,Z,\vartheta) \cdot \Delta\vartheta \leq R \leq \frac{2\pi}{\sigma\,(E,Z)} \sum_o^{i+1} \frac{d\sigma}{d\Omega}\,(E,Z,\vartheta) \cdot \Delta\vartheta$$

with $\frac{d\sigma}{d\Omega}\,(E,Z,\vartheta)$ being the differential scattering cross-section, either for elastic scattering $\frac{d\sigma}{d\Omega}_{Rayleigh}$ or for inelastic scattering $\frac{d\sigma}{d\Omega}_{Compton}$ and R is a random number between 0 and 1.

After an interaction, the resulting ray is traced further using the same process described above, with the current voxel serving as the first voxel potentially interacting with the X-ray. As soon as a ray hits a voxel which is out of bounds of the sample, it is checked whether it hits the entrance window of the second polycapillary optic. Only rays reaching the secondary polycapillary and the detector are currently of interest to the calculation and a new ray is generated or taken from the list and traced through the sample if the entrance window of the secondary polycapillary optic is not reached. The number of times a new ray is generated or taken is logged for each given ray in a predefined number of rays reaching the secondary polycapillary entrance window. This number is called respawns in the following discussion. A flowchart of this process is shown in Fig. 4.

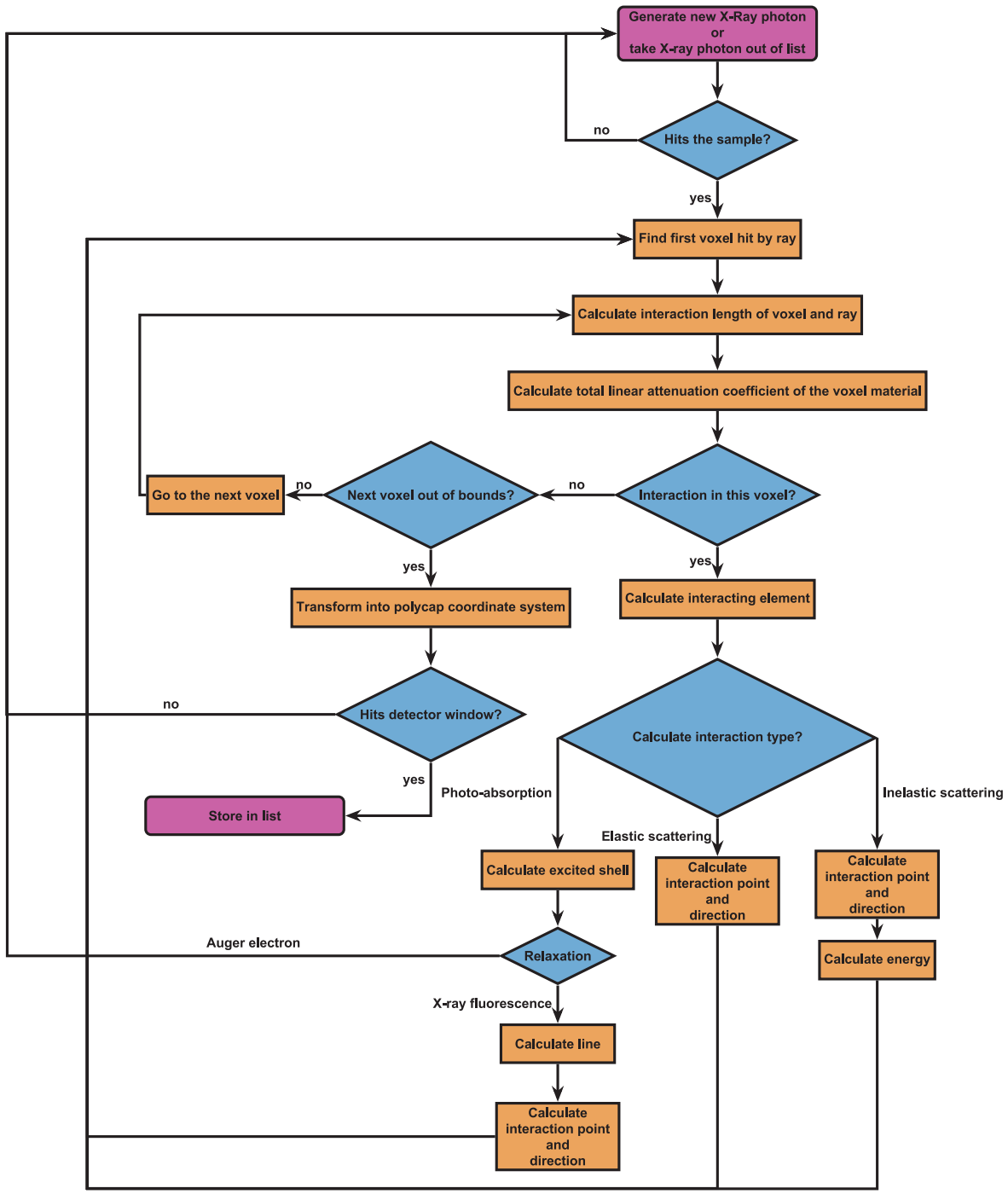

Fig. 4. Flowchart depicting the workflow of voxTrace. X-rays are traced through a sample of given elemental distribution. New primary X-rays are generated or taken from a list of rays until enough scattered and fluorescence photons reach the entrance window of the secondary polycapillary optic.

3. Illustrative examples

To confirm the accuracy of the simulation process, simulated depth scans were compared with empirical results of heavy-matrix and light-matrix samples. All measurements were conducted with the CMXRF setup described in [15]. The heavy-matrix sample NIST 1107 was measured in the lab, using a Mo-anode as the excitation source, with a monochromatic excitation energy of Mo-Kα at 17.4 keV. The light-matrix sample was a 3D-Printed Triple-Cross (Cr-Co-Zn) and was measured with the same setup at the B16 Test Beamline at the Diamond Light Source, using a monochromatic excitation energy of 10 keV [16].

3.1. Naval Brass (NIST 1107)

The NIST 1107 naval brass sample is a well-classified standard reference material. It is a homogeneous material with a certified composition as shown in Table 1.

A sample with a material of the given composition (see Table 1) and a voxel-size of 5 μm $\times$5 μm $\times$5 μm was defined, and a depth scan with a step size of 10 μm simulated. A sufficient signal for the comparison of the main elements Cu and Zn was calculated on a regular workstation PC with an AMD Ryzen 7 5800X, 8C/16T, 3.80–4.70 GHz CPU and a ZOTAC Gaming GeForce RTX 3060 Ti Twin Edge OC LHR, 8 GB GPU in approximately 5 h

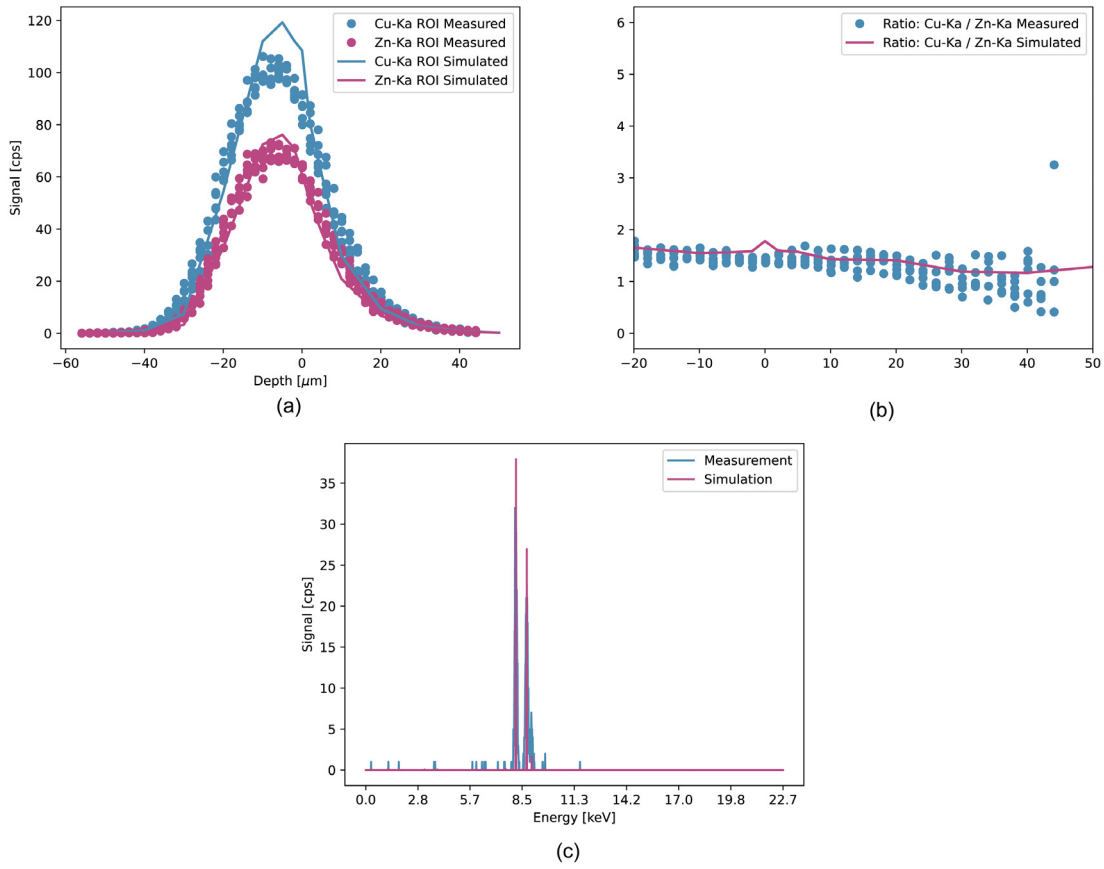

Fig. 5. Comparison of empirical results with simulated data for the standard reference material sample NIST 1107. (a): Plot of the Kα-lines of the main elements Cu and Zn as a function of depth. (b): Signal ratio of the Kα-lines of the main elements Cu and Zn as a function of depth. (c): Measured spectrum for the measurement point in depth 20 μm below sample surface compared to the scaled simulated spectrum in the same measurement point.

Table 1
Elemental Composition of the standard reference material NIST 1107 naval brass as given by the producer.

Element	Mass fraction %
Cu	61.183 ± 0.074
Fe	0.0389 ± 0.0032
Pb	0.1850 ± 0.0024
Ni	0.0946 ± 0.0037
Sn	1.066 ± 0.015
Zn	37.396 ± 0.095

Table 2
Mass fractions of the doping materials of the resin of the layers of a 3D printed reference material.

Layer	Element	Mass fraction %
1	Cr	0.0348
2	Co	0.0456
3	Zn	0.0621

for 20 measurement points. The same results were calculated in approximately 5 min on a single node of the Vienna Scientific Cluster with 2 NVIDIA A40 GPUs and a dual socket with 8 cores AMD EPYC 7252. As a normalization factor representing the primary intensity, the number of respawns necessary for each ray reaching the secondary polycapillary window was used. As shown in Fig. 5, the simulated and empirical results are in good agreement with each other, resulting in a similar ratio of the intensities of the investigated elements, Cu and Zn, in each measurement and simulation position (see Fig. 5). For a perfectly aligned setup the simulated curves seen in Fig. 5 (a), show a much more pointed peak. To obtain the more gaussian shape of the depth curves a small misalignment of the setup was introduced to the simulation. The curves in Fig. 5(a) were calculated with the secondary polycapillary optical axis being tilted 0.1° with respect to a 90° angle between polycapillary optics. Furthermore, the focal point of the secondary polycapillary optic was set at a distance of 10 μm along its own optical axis from the focal point of the primary polycapillary optic. Such a misalignment can be considered small and is difficult to fully eliminate during adjustment of the setup. While such a misalignment might not be perfectly accurate, it shows that manufacturing and adjustment imperfections of the polycapillary can have an influence on the shape of the depth curve.

3.2. 3D-Printed Triple-Cross (Cr-Co-Zn)

An ongoing challenge in the field of CMXRF is the lack of adequate standard materials with a three-dimensional structure. To tackle this problem, we developed and investigated samples created with a stereo lithography 3D-printer. The base material is a liquid photopolymer resin that cures when exposed to ultraviolet light. Resins doped with different metals were used to print a three-dimensional structure with well-defined elemental distribution. Table 2 shows the mass fractions of the added metal in the different layers. Fig. 6 shows a microscope image of the printed structure and the comparison of simulated and measurement signal curve for the added materials for a depth scan of the sample.

For the simulation of a depth scan for this sample, the materials in each layer were modelled using the mass fractions given in

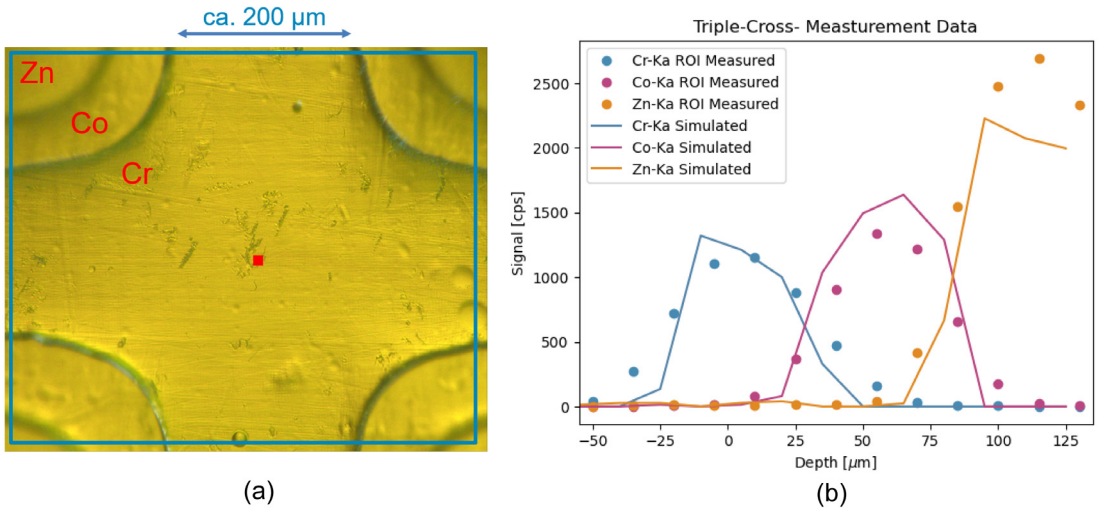

Fig. 6. 3D-printed triple-cross structure (Cr-Co-Zn). Each layer was printed using resins doped with different metals to print a three-dimensional structure with well-defined elemental distribution (a): Microscope image. (b): Plot of the Kα-lines of the elements Cr, Co and Zn as a function of depth.

Table 2 and the rest of the mass modelled as pure carbon. While this model is not perfectly accurate, the measured and simulated curves show good agreement (Fig. 6).

Both heavy- and light-matrix samples show good agreement between simulated and measured spectra and depth curves, showing the validity of the simulation, for this kind of samples. Effects of secondary excitation are considered in the simulation process, yet very small for the given sample, due to the low concentrations of the doping elements in the sample. The development of fitting reference materials for further validation of the software can be facilitated by simulation of layer systems of different compositions, thus calculating minimal concentration for which discernible effects are to be expected.

4. Impact

CMXRF is a widely used technique for the investigation of the three-dimensional elemental distribution of samples using both laboratory and synchrotron X-ray sources. Quantitative interpretations of such measurements are often of interest but difficult to obtain. A reason for this is the high effort required in producing good reference materials, as well as the high computational demands of solving these problems, which must consider the energy dependent transmission properties of polycapillary half-lens optics, and the absorption and scattering effects inside the sample.

The full ray-tracing approach of voxTrace allows the investigation of these effects, such as higher order excitation and scattering. A further benefit of this new approach is the possibility to skip the peak deconvolution process of the measured spectra, as simulation results can be used to generate spectra directly, which can then be fitted to measured spectra. This is especially important and helpful for materials with overlapping fluorescence peaks. Furthermore, absorption effects can lead to deviation from tabulated line ratios and make the peak deconvolution process difficult and faulty.

A further improvement of this software is its time efficiency. Given sufficient resources, exact simulations of all relevant radiation-matter interactions in the sample can be simulated within reasonable timescales. In combination with global optimization algorithms, which we aim to implement in the near future, the exact quantitative evaluation of CMXRF spectra will be possible, without estimations about the confocal volume and without computationally expensive reconstruction algorithms. While the exact computing time depends on the nature of the sample and the experimental setup, as well as the computing setup, it has been shown that a feasible simulation time can be achieved for a statistically relevant signals, for samples with a heavy matrix and with a light matrix, both on a reasonably priced computer system and a high-performance cluster.

As voxTrace is brand-new software its user group is currently small. Hopefully, the use of the software will be spread to multiple institutions practising CMXRF techniques, including synchrotron beamlines and research groups with lab-based CMXRF setups.

5. Conclusions

In this paper we demonstrated that voxTrace software is an adequate tool for the simulation of energy dispersive XRF spectra obtained in typical CMXRF setups. The use of general-purpose computing on graphics processing units (GPGPU) proved to be well-suited for the computationally expensive task of tracing rays through a sample and simulating the relevant radiation-matter interactions. Simulated spectra and depth-intensity curves are in good agreement with measurements of light-matrix and heavy-matrix samples, showing the validity of the software, for the investigated samples.

Important features of the voxTrace software are an energy independent voxel size of the sample allowing the modelling of surfaces and scans with a step size smaller than the confocal volume. Therefore, an investigation of samples with higher accuracy is possible. Furthermore, higher order effects, such as secondary excitation, can be investigated using voxTrace. The development of suiting 3D standard reference materials will utilize this simulation of secondary excitation effects. The process of directly simulating spectra, instead of peak deconvolution of single spectra and processing absorption effects independently, can be advantageous for the investigation of samples with materials with overlapping line energies. Furthermore, the peak deconvolution for heavy matrix samples can be difficult, as absorption effects lead to deviation from tabulated line ratios.

In future development, the implementation of global optimization algorithms will allow an iterative optimization of the difference between simulated and measured spectra by varying the elemental distribution of different voxels and, therefore, the

quantitative interpretation of CMXRF measurements. This is made feasible by the acceleration of the vast parallelization capabilities of GPUs.

Declaration of competing interest

The authors declare that they have no known competing financial interests or personal relationships that could have appeared to influence the work reported in this paper.

Data availability

Data will be made available on request.

Acknowledgements

The authors would like to thank Diamond Light Source for beamtime (proposal MM29861) and the principal beamline scientist of beamline B16 (Kawal Sawhney) for support.

The computational results presented have been achieved in part using the Vienna Scientific Cluster (VSC). We thank Markus Hickel from the VSC-Team for his support.

The authors acknowledge TU Wien Bibliothek, Austria for financial support through its Open Access Funding Programme.

References

[1] Nakano K, Nishi C, Otsuki K, Nishiwaki Y, Tsuji K. Depth elemental imaging of forensic samples by confocal micro-XRF method. Anal Chem 2011;83(9):3477–83. http://dx.doi.org/10.1021/ac1033177.

[2] Eveno M, Mysak E, Müller K, Bastian G, Pincas N, Reiche I. Confocal XRF depth profiling nondestructively reveals the original blue pigments in a renaissance painting by Caroto. Stud Conserv 2016;61(2):102–12. http://dx.doi.org/10.1080/00393630.2016.1142059.

[3] Kanngiezer B, Malzer W, Mantouvalou I, Sokaras D, Karydas A. A deep view in cultural heritage—confocal micro X-ray spectroscopy for depth resolved elemental analysis. Appl Phys A 2011;106(2):325–38. http://dx.doi.org/10.1007/s00339-011-6698-0.

[4] Iro M, Ingerle D, Radtke M, Guilherme Buzanich A, Kregsamer P, Streli C. Investigation of polycapillary half lenses for quantitative confocal micro-X-ray fluorescence analysis. J Synchrotron Radiat 2022;29(6):1376–84. http://dx.doi.org/10.1107/s1600577522009699.

[5] Förste F, et al. Quantification routines for full 3D elemental distributions of homogeneous and layered samples obtained with laboratory confocal micro XRF spectrometers. J Anal At Spectrom 2022;37(8):1687–95. http://dx.doi.org/10.1039/d2ja00119e.

[6] Sanchez Del Rio M, Canestrari N, Jiang F, Cerrina F. SHADOW3: A new version of the synchrotron X-ray optics modelling package. J Synchrotron Radiat 2011;18(5):708–16. http://dx.doi.org/10.1107/S0909049511026306.

[7] Tack P, Schoonjans T, Bauters S, Vincze L. An X-ray ray tracing simulation code for mono- and polycapillaries: Description, advances and application. Spectrochim Acta - Part B At Spectrosc 2020;173(July):105974. http://dx.doi.org/10.1016/j.sab.2020.105974.

[8] Brunetti A, Sanchez Del Rio M, Golosio B, Simionovici A, Somogyi A. A library for X-ray-matter interaction cross sections for X-ray fluorescence applications. Spectrochim Acta - Part B At Spectrosc 2004;59(1725). http://dx.doi.org/10.1016/j.sab.2004.03.014, 10–11–1731.

[9] Schoonjans T, et al. The xraylib library for X-ray-matter interactions. Recent developments. Spectrochim Acta - Part B At Spectrosc 2011;66(11–12):776–84. http://dx.doi.org/10.1016/j.sab.2011.09.011.

[10] Vincze L, Janssen K, Adams F. A general Monte Carlo simulation of energy-dispersive X-ray fluorescence spectrometers-I. Unpolarized radiation, homogeneous samples. Spectrochim Acta Part B At Spectrosc 1993;48(4):553–73. http://dx.doi.org/10.1016/0584-8547(93)80060-8.

[11] Vincze L, Janssens K, Adams F, Rivers ML, Jones KW. A general Monte Carlo simulation of ED-XRF spectrometers. II: Polarized monochromatic radiation, homogeneous samples. Spectrochim Acta Part B At Spectrosc 1995;50(2):127–47. http://dx.doi.org/10.1016/0584-8547(94)00124-E.

[12] Vincze L, Janssens K, Adams FC, Jones KW. A general Monte Carlo simulation of energy-dispersive X-ray fluorescence spectrometers. Part 3. Polarized polychromatic radiation, homogenous samples. Spectrochim Acta 1995;50:1481–500. http://dx.doi.org/10.1016/0584-8547(95)01361-X.

[13] Schoonjans T, et al. A general Monte Carlo simulation of energy dispersive X-ray fluorescence spectrometers - Part 5: Polarized radiation, stratified samples, cascade effects, M-lines. Spectrochim Acta - Part B At Spectrosc 2012;70:10–23. http://dx.doi.org/10.1016/j.sab.2012.03.011.

[14] Schoonjans T, Solé VA, Vincze L, Sanchez Del Rio M, Appel K, Ferrero C. A general Monte Carlo simulation of energy-dispersive X-ray fluorescence spectrometers - Part 6. Quantification through iterative simulations. Spectrochim Acta - Part B At Spectrosc 2013;82:36–41. http://dx.doi.org/10.1016/j.sab.2012.12.011.

[15] Ingerle D, Swies J, Iro M, Wobrauschek P, Streli C, Hradil K. A monochromatic confocal micro-x-ray fluorescence (μXRF) spectrometer for the lab. Rev Sci Instrum 91(12):2020. http://dx.doi.org/10.1063/5.0028830.

[16] Dolbnya IP, et al. A water-cooled monochromator for the B16 test beamline at the diamond light source: capabilities and performance characterization. J Synchrotron Radiat 2019;26(1):1. http://dx.doi.org/10.1107/S1600577518014662.